



**Universiteit  
Leiden**  
The Netherlands

## **A multimodal, comprehensive characterization of a cutaneous wound model in healthy volunteers**

Voorde, W. ten; Saghari, M.; Boltjes, J.; Kam, M.L. de; Zhuparris, A.; Feiss, G.; Buters, T.P.; ... ; Rissmann, R.











### **Citation**

Voorde, W. ten; S. , M., Boltjes, J., Kam, M. L. de, Zhuparris, A., Feiss, G., Buters, T. P., ... Rissmann, R. (2023). A multimodal, comprehensive characterization of a cutaneous wound model in healthy volunteers. *Experimental Dermatology*, 32(7), 1028-1041.  
doi:10.1111/exd.14808

Version: Publisher's Version  
License: [Creative Commons CC BY-NC 4.0 license](#)  
Downloaded from: <https://hdl.handle.net/1887/3620370>

**Note:** To cite this publication please use the final published version (if applicable).

# A multimodal, comprehensive characterization of a cutaneous wound model in healthy volunteers

Wouter ten Voorde<sup>1,2</sup>  | Mahdi Saghari<sup>1,2</sup>  | Jiry Boltjes<sup>1</sup> | Marieke L. de Kam<sup>1</sup> | Ahnjili Zhuparris<sup>1</sup>  | Gary Feiss<sup>3</sup> | Thomas P. Buters<sup>1,2</sup>  | Errol P. Prens<sup>4</sup>  | Jeffrey Damman<sup>5</sup>  | Tessa Niemeyer-van der Kolk<sup>1</sup>  | Matthijs Moerland<sup>1</sup> | Jacobus Burggraaf<sup>1,2,6</sup>  | Martijn B. A. van Doorn<sup>3</sup>  | Robert Rissmann<sup>1,2,6</sup> 

<sup>1</sup>Centre for Human Drug Research, Leiden, the Netherlands

<sup>2</sup>Leiden University Medical Centre, Leiden, the Netherlands

<sup>3</sup>Cutanea Life Sciences, Wayne, Pennsylvania, USA

<sup>4</sup>Department of Dermatology Erasmus Medical Centre, Rotterdam, the Netherlands

<sup>5</sup>Department of Pathology Erasmus Medical Centre, Rotterdam, the Netherlands

<sup>6</sup>Leiden Academic Center for Drug Research, Leiden University, Leiden, the Netherlands

## Correspondence

Robert Rissmann, Centre for Human Drug Research, Leiden, the Netherlands.  
Email: [rissmann@chdr.nl](mailto:rissmann@chdr.nl)

## Funding information

Cutanea Life Sciences

## Abstract

Development of pharmacological interventions for wound treatment is challenging due to both poorly understood wound healing mechanisms and heterogeneous patient populations. A standardized and well-characterized wound healing model in healthy volunteers is needed to aid in-depth pharmacodynamic and efficacy assessments of novel compounds. The current study aims to objectively and comprehensively characterize skin punch biopsy-induced wounds in healthy volunteers with an integrated, multimodal test battery. Eighteen (18) healthy male and female volunteers received three biopsies on the lower back, which were left to heal without intervention. The wound healing process was characterized using a battery of multimodal, non-invasive methods as well as histology and qPCR analysis in re-excised skin punch biopsies. Biophysical and clinical imaging read-outs returned to baseline values in 28 days. Optical coherence tomography detected cutaneous differences throughout the wound healing progression. qPCR analysis showed involvement of proteins, quantified as mRNA fold increase, in one or more healing phases. All modalities used in the study were able to detect differences over time. Using multidimensional data visualization, we were able to create a distinction between wound healing phases. Clinical and histopathological scoring were concordant with non-invasive imaging read-outs. This well-characterized wound healing model in healthy volunteers will be a valuable tool for the standardized testing of novel wound healing treatments.

## KEYWORDS

drug development, healthy volunteers, non-invasive imaging, skin punch biopsy, wound healing model

This is an open access article under the terms of the [Creative Commons Attribution-NonCommercial](https://creativecommons.org/licenses/by-nc/4.0/) License, which permits use, distribution and reproduction in any medium, provided the original work is properly cited and is not used for commercial purposes.

© 2023 The Authors. *Experimental Dermatology* published by John Wiley & Sons Ltd.

## 1 | INTRODUCTION

Cutaneous trauma as induced by a cut or burn of the skin initiates a cascade of phasic events to restore the skin's function. Classically, the phases of wound healing are referred to as haemostasis, inflammation, proliferation and remodeling (Figure 1A), where each phase elicits a peak activity at a certain time in the wound healing cascade (arbitrarily depicted in Figure 1A).<sup>1–4</sup> The phases are marked by signalling pathways mediated by numerous cell types, growth factors and cytokines under normal conditions.<sup>5,6</sup> After haemostasis, each subsequent phase is characterized by changes in the microenvironment including the secretion of cytokines and chemokines, and the attraction, migration and activation of various cell types.<sup>7</sup> In addition, the microbiome is thought to play an important role in wound healing.<sup>8</sup> In delayed wound healing and chronic wounds, the typical cascade is impaired, mainly in the inflammation phase.<sup>9</sup> For these situations, an intervention for improved and accelerated wound healing is desirable.

Currently no clear consensus has been reached regarding the most important factors resulting in delayed healing in humans and how to improve or accelerate wound healing.<sup>10</sup> Lack of insight into the mechanisms and processes of wound healing has hindered the development of new interventions and therapies.<sup>11,12</sup> The heterogeneity of wounds related to complex comorbidities and differences in wound induction (i.e. acute wound, burn wound, cut wound, chronic wound) creates challenges. The need to find effective treatment options for acute and chronic wounds is unmet. The financial burden to treat chronic wounds is estimated to be approximately \$ 15–22 billion by the end of 2024.<sup>13,14</sup> In the last five years, only a limited number of clinical trials have been performed focusing on a novel treatment for wounds using an evidence-based approach. One contributing factor may be the lack of a robust human wound healing model for early phase clinical studies.<sup>15,16</sup> The current standard endpoint to evaluate wound healing (also used by regulators) is based on time to complete healing, and focusses on the wound visible with the naked eye.<sup>17</sup> A more in-depth human wound healing model using healthy volunteers had been introduced earlier.<sup>18,19</sup> However, while the model had shown that optical coherence tomography (OCT) is capable of distinguishing cutaneous structural changes and that the measurement was comparable to histology, the focus rested on the non-invasive nature of this device alone. A full integration of modalities to changes in the skin's structure, function and microenvironment could aid in wound healing drug development.

To address these challenges, a study was designed with the aim to comprehensively characterize the mechanisms and processes of physiological wound healing. A standardized 3mm full-thickness skin punch biopsy on the back of healthy volunteers was made and measured with a standardized, multimodal test battery yielding a multidimensional approach.<sup>20,21</sup> All healing phases after haemostasis were extensively, (non)-invasively characterized in different domains, that is biophysical, cellular, molecular, clinical aspects and clinical imaging. Methods with objective and biomarker-based readout were deployed as depicted in Figure 1A,C. Finally, the data were

integrated using advanced data visualization techniques to fully exploit this high-temporal and high-spatial resolution data set.

## 2 | MATERIALS AND METHODS

This was a prospective single-arm, biopsy-location randomized, observational study in healthy volunteers performed at the Centre for Human Drug Research, Leiden, The Netherlands (NL63280.056.17). The trial was executed in accordance with the declaration of Helsinki. The independent Medical Review and Ethics Committee 'Medisch Ethische Toetsingscommissie van de Stichting Beoordeling Ethiek Biomedisch Onderzoek' (Assen, the Netherlands) approved the study prior to clinical study activities. All subjects received oral and written information and gave written informed consent before participation. The study lasted from November 2017 till March 2018. The trial was registered on [ClinicalTrials.gov](https://clinicaltrials.gov) (NCT03433820).

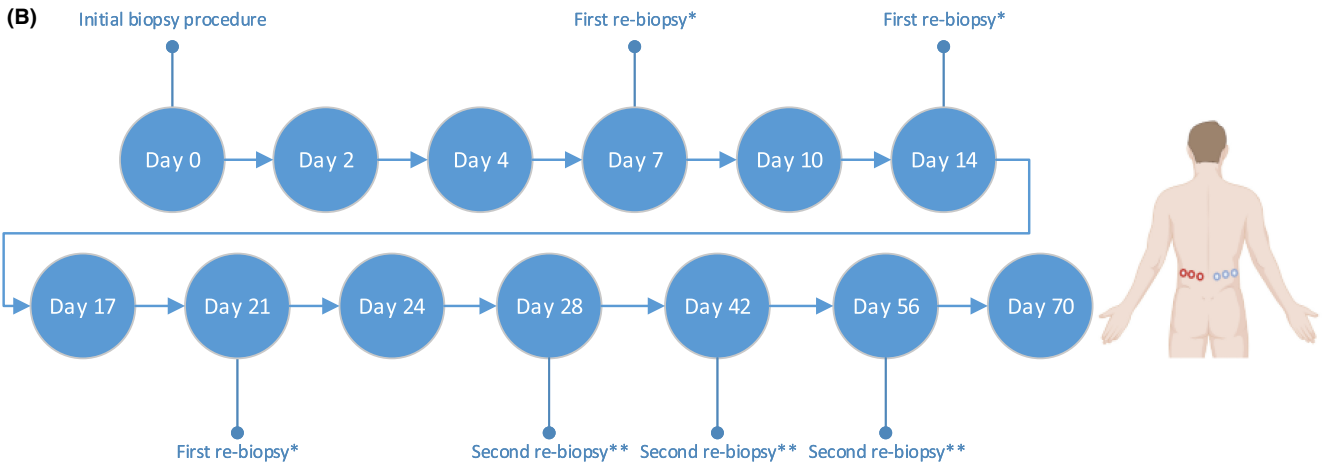
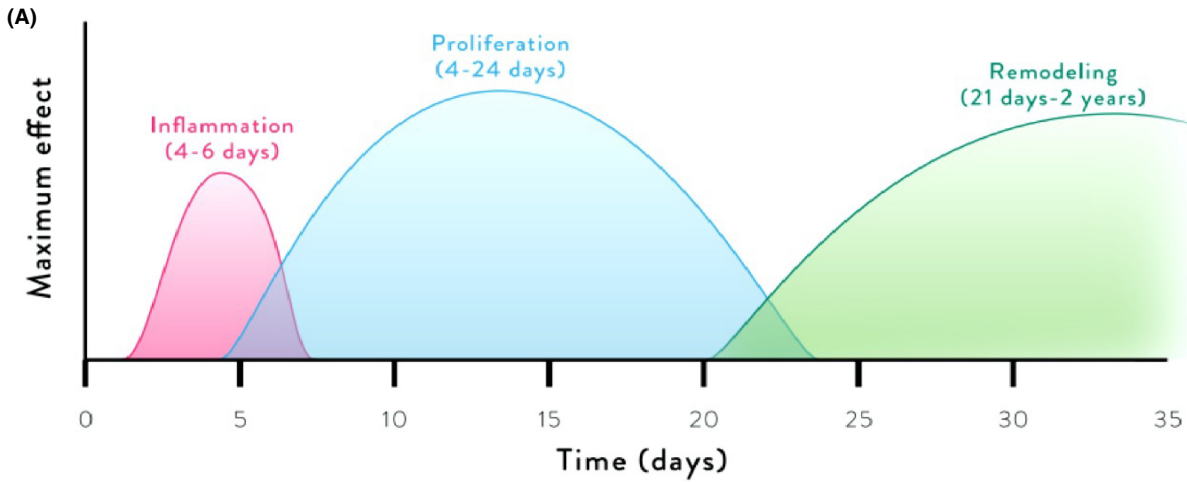
### 2.1 | Subjects, study design and randomization

In total, 18 non-smoking healthy male and female volunteers (Fitzpatrick skin type I–II), aged 18–30 years with a body mass index (BMI) between 18 and 30 kg/m<sup>2</sup> were included. Main exclusion criteria were history of pathological scar formation, smoking, clinically relevant skin conditions and diseases associated with immunosuppressive or immunomodulatory medication. Overall health status was assessed by physical examination, electrocardiogram (ECG), blood pressure measurements and blood analysis.

An overview of the wound healing phases used to classify the data and the trial design are depicted in Figure 1A,B. All subjects underwent three full-thickness skin punch biopsies (3mm) on the lower back on the first study day, which were randomly performed on the right or left side of the lower back. After the biopsy procedure, the wounds were covered with gauze dressing until haemostasis was completed. After haemostasis the wounds were left untreated and uncovered. Subjects were randomized to receive two repeated biopsies on day 7, 14 or 21 and on day 28, 42 or 56 ( $n=6$  per repeated biopsy day), respectively. For all imaging, clinical and biophysical parameters eighteen 3mm biopsy wounds were followed over time. For all molecular and cellular parameters eighteen 3mm biopsy wounds were measured on day 0, and six 4mm biopsy wounds were measured on subsequent timepoints.

### 2.2 | Biophysical: skin blood perfusion and skin barrier function

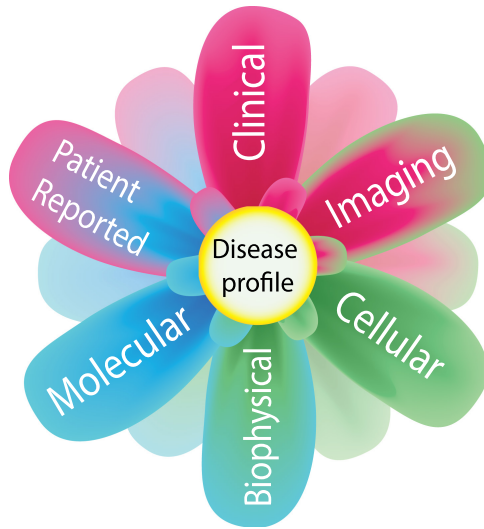
Skin blood perfusion was quantified using Dynamic Optical Coherence Tomography (D-OCT; VivoSight OCT, Michelson diagnostics) at baseline and on each study day visit as described before.<sup>22,23</sup> Subjects were acclimatized to a temperature-controlled room and lighting was kept constant for the entire duration of the



- (C) Clinical
- › Erythema grading scale (EGS)
  - › Target lesion scores (POSAS)

Patient reported  
 Adverse event reporting ‹  
 Symptom reporting (NRS) ‹  
 Concomitant medication ‹

Molecular  
 Transcriptomics (qPCR) ‹  
 Immunohistochemistry ‹



Imaging  
 › Clinical photography  
 › Planimetry (3D imaging)  
 › Colorimetry (multispectral imaging)  
 › Morphology (optical coherence tomography)

Cellular  
 › Histology

Biophysical  
 › Trans-epidermal water loss  
   › Thermography  
 › Skin perfusion (laser speckle)

**FIGURE 1** (A) Schematic representation of wound healing phases. Phase separation into set days is arbitrary and can differ dependant on the wound. (B) Clinical study design. Three-times 3 mm biopsies were taken on day 0 either on the right or left side of the lower back and were left to heal without intervention. \*Subjects were randomized to receive the first 4 mm re-biopsy on day 7, day 14 or day 21. \*\*Subjects were randomized to receive the second 4 mm re-biopsy on day 28, day 42 or day 56. (C) Blueprint for mechanistic and clinical pharmacology studies. Adapted from Rissmann et al. (2020). All assessments are reported in this article.

trial. D-OCT recordings were captured using a 6 mm probe placed directly over the wound creating a closed environment between skin and laser. 120 consecutive scans with a depth of up to 1.5 mm were taken of the wounds in approximately 20s. Cutaneous microcirculation was quantified by calculating the average speckle signal returning from a depth of 0.1 mm up to 0.35 mm to reduce artefacts and noise signal.<sup>24</sup>

Skin barrier function was measured using transepidermal water loss measurements (TEWL; Aquaflux AF200, Biox Systems). Subjects were acclimatized to the room for 15 min before the start of a measurement. A probe was placed on the wound creating a closed chamber of 3 mm, after which a measurement was started. Humidity differences between the TEWL chamber and the skin results in movement of water particles. Sensors in the chamber detect the water particles over time. A measurement lasted for 90 seconds or until steady-state flux was reached.

### 2.3 | Clinical imaging: erythema, planimetry and morphology

Skin erythema was quantified using multispectral imaging (Antera 3D®, Miravex), as described in detail before.<sup>22,23,25</sup> The multispectral camera creates a closed chamber of 25 cm<sup>2</sup> for image capture with standardized lighting and distance. A region of interest of 4 mm in diameter was defined and kept analogous with all analysed images. Skin erythema was defined as the  $a^*$  value (AU) using the CIE Lab colour classification system.<sup>26</sup>

Planimetry (volume, surface, depth) of the induced wounds was measured using a stereophotogrammetric 3D camera (LifeViz 3D®, Quantificare).<sup>27</sup> Two 2D images were created simultaneously using a parallel lensing system. Standardized lighting and distance were established by flash, a light-controlled room and guidance lasers. Standardized pictures were taken on all study day visits. Images were analysed using accompanying software (DermaPix®, Quantificare). The inner wounds (wounds without perilesional elevation/depression of skin included) were traced by a single experienced analyst. Analysis was performed only when a wound was present. Depth, surface and volume were reported in mm, mm<sup>2</sup> and mm<sup>3</sup>, respectively. Volume was calculated using an algorithm based on volume calculations for a cone.

Qualitative assessment of the skin's morphology was performed using Optical Coherence Tomography (OCT; VivoSight, Michelson Diagnostics Ltd). A 6 mm probe was placed directly over the wound and recorded 120 consecutive images in approximately 20s. Recordings were up to 1.5 mm in depth and reached a lateral and spatial resolution of 7.5 and 5 μm, respectively. Qualitative

inspection of the images was performed by two experienced observers and quantitative analysis comprised automated epidermal thickness measurements. Epidermal thickness was calculated by subtracting the signal corresponding to the change from epidermis to dermis (dermo-epidermal junction) from the signal corresponding to the transition from air to skin.

### 2.4 | Molecular & cellular: skin punch biopsies

Three- and four-millimetre skin punch biopsies were snap frozen in liquid nitrogen directly after harvest. Biopsies were stored at ≤−80°C until shipment and analysed at the Immunology Laboratory of Erasmus Medical Center, Rotterdam, The Netherlands. mRNA extraction was performed using GenElute™ Mammalian Total RNA Miniprep kit (Sigma Aldrich™, RTN350-1KT) and expression was determined for CTGF, EGF, FGF1, FGF2, GM-CSF, IL-6, IL-10, IL-33, IL-1β, MMP1, MMP3, MMP9, PDGFA, PDGFB, PGF, TGF-β1, TGF-β3, TNF, VEGF-A relative to the housekeeping gene ABL using quantitative reverse transcriptase polymerase chain reaction (RT-qPCR, ViiA™ 7 Real-Time PCR system). Furthermore, biopsies were haematoxylin-eosin stained to compare with time-matched OCT recordings and clinical images. Histopathological scores were graded by an independent histopathologist. Histopathology scores were given to 5 healing parameters (wound re-epithelialization, granulation tissue, inflammation, neoangiogenesis and connective tissue formation) with corresponding assessment parameters and were graded from 0–3 corresponding to absent, scant, moderate and profound, respectively. To evaluate the wound healing over time, re-biopsies were used in the histopathologist scoring, as reported earlier.<sup>28</sup>

### 2.5 | Clinical: red-yellow-black, erythema grading scale and patient observer scar assessment scores

Clinical scores of the wounds were performed using the red-yellow-black (RYB) score, erythema grading scale (EGS) and Patient Observer Scar Assessment Scores (POSAS) as described before.<sup>29–31</sup> All scores were performed by a single trained physician. The RYB score consisted of three wound parameters: wound presence, wound colour and wound humidity. RYB scores were only completed on days that a wound was present. EGS scores were graded absent, mild, moderate or severe and were performed on all study day visits. POSAS scores were only performed when the wound was closed. Since the wounds were created on the lower back only the observer scores of the POSAS were performed.

## 2.6 | Data visualization

An exploratory data analysis and visualization of the wound healing data was performed to identify distinct wound healing phases. To visualize if the different wound healing phases could be clustered based on the objective wound healing parameters, the data was projected into a t-distributed Stochastic Neighbour Embedding (t-SNE) space using the Python (Python Software Foundation) package scikit-learn version 1.0.2. t-SNE is an effective non-linear dimensionality reduction technique used to create a two-dimensional representation of a high dimensional dataset to visualize and identify potential clusters.<sup>32</sup> Data from all timepoints were arbitrarily divided over three phases based on literature.<sup>33-36</sup> The inflammation phase lasted from day 2 to day 7, the proliferation phase from day 10 to day 24 and the remodeling phase from day 28 to day 70. Data from day 0 was used as healthy pre-challenged skin.

For further visual comparison of categorical groups across multiple quantitative parameters a radar chart was developed. The magnitude of the parameter for each data point in relation to the maximum magnitude of the parameter across all the data points was calculated using Python (Python Software Foundation) and classified using the wound healing phases depicted in [Figure 1A](#).<sup>37</sup>

## 2.7 | Statistics

All statistical and randomization programming was performed by a study-independent statistician and created using SAS 9.4 software (SAS Institute Inc.). Biopsies were randomly performed using a randomization list with order of biopsy codes. The randomization code was only made available after study completion. For all physical, imaging and clinical parameters data are summarized and displayed and reported descriptively (mean  $\pm$  SD).

## 3 | RESULTS

A total of thirty-two (32) volunteers were screened for participation in the study. Fourteen (14) volunteers were excluded based on inclusion/exclusion criteria. Nine (50%) male and nine (50%) female Caucasian subjects participated in this trial ([Table 1](#)). No serious adverse events (SAEs) or discontinuation due to AEs occurred. All AEs were of mild severity and self-limiting.

### 3.1 | Skin blood perfusion and skin barrier function restored within 28 days after the initial biopsy

An increased cutaneous microcirculation ([Figure 2A](#)) was observed after the skin punch biopsy procedure as quantified with OCT indicating the start of the inflammation phase ([Figure 2B](#)). The average blood flow peaked at day 2 (mean  $0.11 \pm 0.03$  AU, Phase II) and was elevated up to day 7 (mean  $0.11 \pm 0.03$  AU, Phase II). From day 7

**TABLE 1** Subject demographics and baseline characteristics.

Age (years)	
N	18
Mean (SD)	21.9 (2.0)
Median	22.0
Min, Max	18, 25
Height (cm)	
N	18
Mean (SD)	176.8 (8.2)
Median	176.9
Min, Max	164.1, 193.5
Weight (kg)	
N	18
Mean (SD)	70.2 (10.2)
Median	70.1
Min, Max	55.3, 91.95
BMI (kg/m <sup>2</sup> )	
N	18
Mean (SD)	22.4 (2.6)
Median	21.8
Min, Max	18.3, 27.9
Sex	
Female	9 (50.0%)
Male	9 (50.0%)
Race	
White	18 (100.0%)
Fitzpatrick skin type	
1 (always burns and never tans)	1 (5.6%)
2 (always burns and tans min)	17 (94.4%)

Abbreviation: BMI, body mass index.

onwards a return to baseline was observed, which completed at day 17 showing the transition from the inflammation to the proliferation phase (mean  $0.05 \pm 0.01$  AU, Phase III).

The skin barrier function represented by TEWL flux levels was highly impaired directly after the skin punch biopsy on day 0 ([Figure 2C](#)). A maximum mean flux of  $61.0 \text{ g/m}^2\text{h}$  was observed on day 2 (Phase II), which decreased over time returning to the baseline value at day 28 (mean  $13.8 \pm 4.1 \text{ g/m}^2\text{h}$ , Phase IV).

### 3.2 | Novel clinical imaging tool can objectively identify differences in size, colour and cutaneous structures of the induced wounds

Erythema of the skin as quantified by multispectral clinical imaging was visible in all wound healing phases starting two days after biopsy procedure (mean  $27.44 \pm 4.16$  AU, Phase II) and remained variably present up to day 70 (mean  $25.39 \pm 2.34$  AU, Phase IV), not returning to the baseline value at end of study ([Figure 3A](#)).



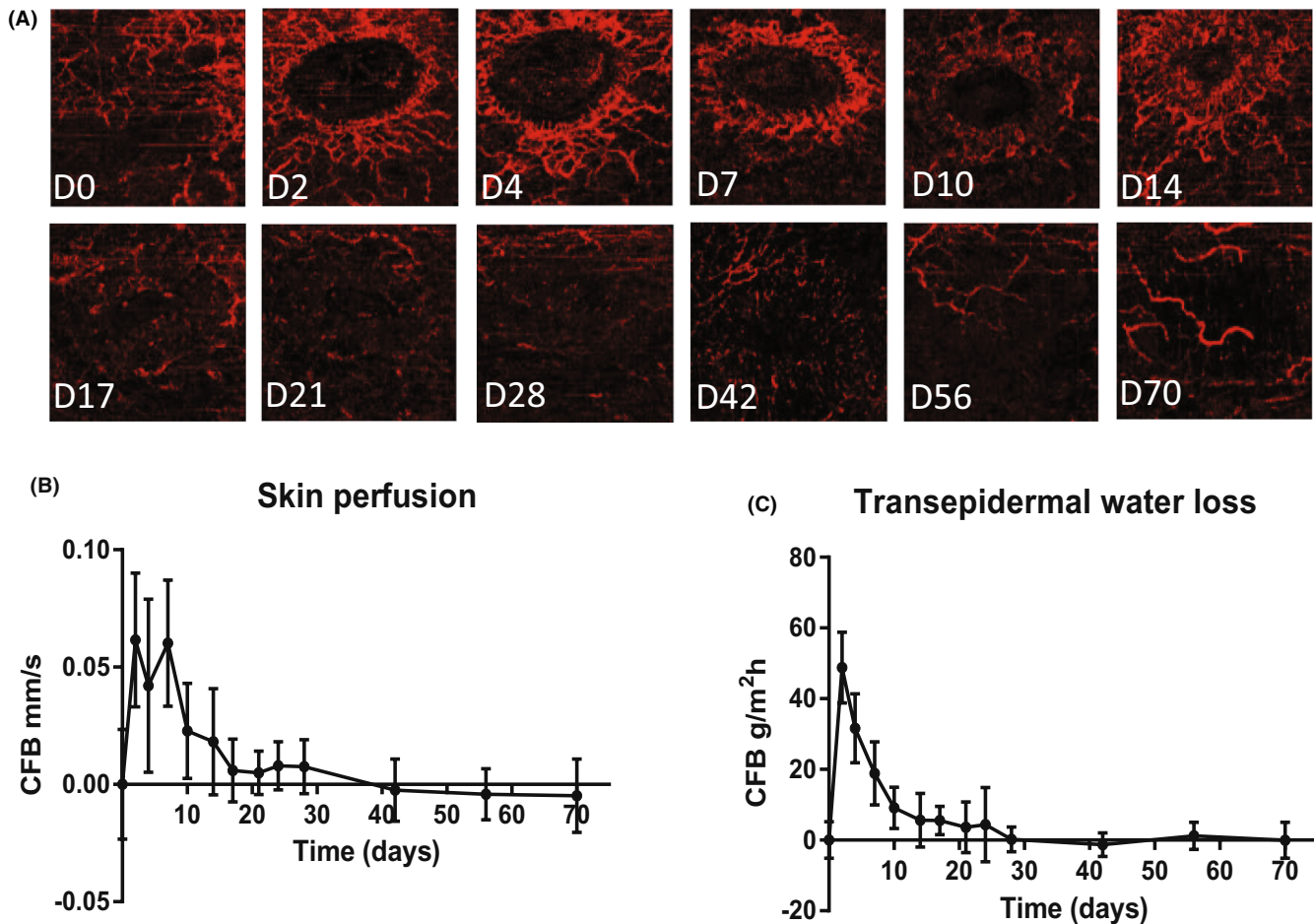


**FIGURE 2** Biophysical response after 3 mm skin punch biopsies over time. (A) representative images of D-OCT skin blood perfusion parameter at a measuring depth of 0.35 mm on the indicated study days. (B) Skin blood perfusion, displayed in change from baseline (day 0) [mm/s] up to day 70, is increased after wounding and gradually decreases over time ( $n = 18$ ). (C) Transepidermal water loss, displayed in change from baseline [g/m<sup>2</sup>h] over time, is increased after wound induction and decreases steeply over time ( $n = 18$ ). All data are expressed as change from baseline, means  $\pm$  standard deviation.

Stereophotogrammetric parameters (volume, surface, depth) are displayed in Figure 3C–E. Two days after biopsy procedure there was a negative wound volume (mean  $-1.32 \pm 0.95$  mm<sup>3</sup>, Phase II), indicating a concave planimetry. From day 2 up to day 10. During the inflammation and proliferation phases (Phase II/III) the wound volume became positive (mean  $0.58 \pm 0.39$  mm<sup>3</sup>), followed by a decrease and return to the pre-biopsy conditions on day 28 (Phase IV). Although no wound was visible anymore after day 28 in the remodeling phase (and no analysis could be performed) a small elevation of the skin was observed upon visual inspection on day 28 and during the following visits.

The initial wounds had a mean surface of  $7.55 \pm 1.24$  mm<sup>2</sup> at day 2 (Phase II). A gradual wound closure was observed from day 2 up to day 24 (mean  $0.11 \pm 0.39$  mm<sup>2</sup>, Phase II/III), with full closure of the wound on day 28 (Phase IV). The mean maximum inner wound depth quantified 2 days after the biopsy procedure (Phase II) was  $-0.41 \pm 0.15$  mm, which returned to a flat and normalized state at day 28 (Phase IV).

Automatically calculated epidermal thickness measurements calculated by OCT showed an increase in epidermal thickness in the

remodeling phase 4 weeks after wounding followed by a gradual decrease over time up to day 70 (Figure 3F). Epidermal thickness did not return to baseline values in 70 days. Epidermal thickness measurements could not be performed on day 7, 10 and 14 due to crust interference and lack of epidermis.

### 3.3 | mRNA expression levels of wound related proteins clearly follow the wound healing phases

The molecular response to skin wounding was studied by quantifying mRNA expression in snap frozen 3- and 4-mm biopsies using qPCR (Figure 4). In general, day 0 data consist of 18 skin punch biopsies, whilst the remaining time points consist of 6 skin punch biopsies due to the randomized procedure for repeated biopsies. The inflammation phase (Phase II) was characterized by the upregulation of several pro-inflammatory cytokines between day 0 and 7 (i.e. IL-1 $\beta$ , IL-10, IL-33, TNF, GM-CSF, VEGF-A) followed by a decrease and stabilization at day 28 (Figure 4A–E). mRNA expression levels of

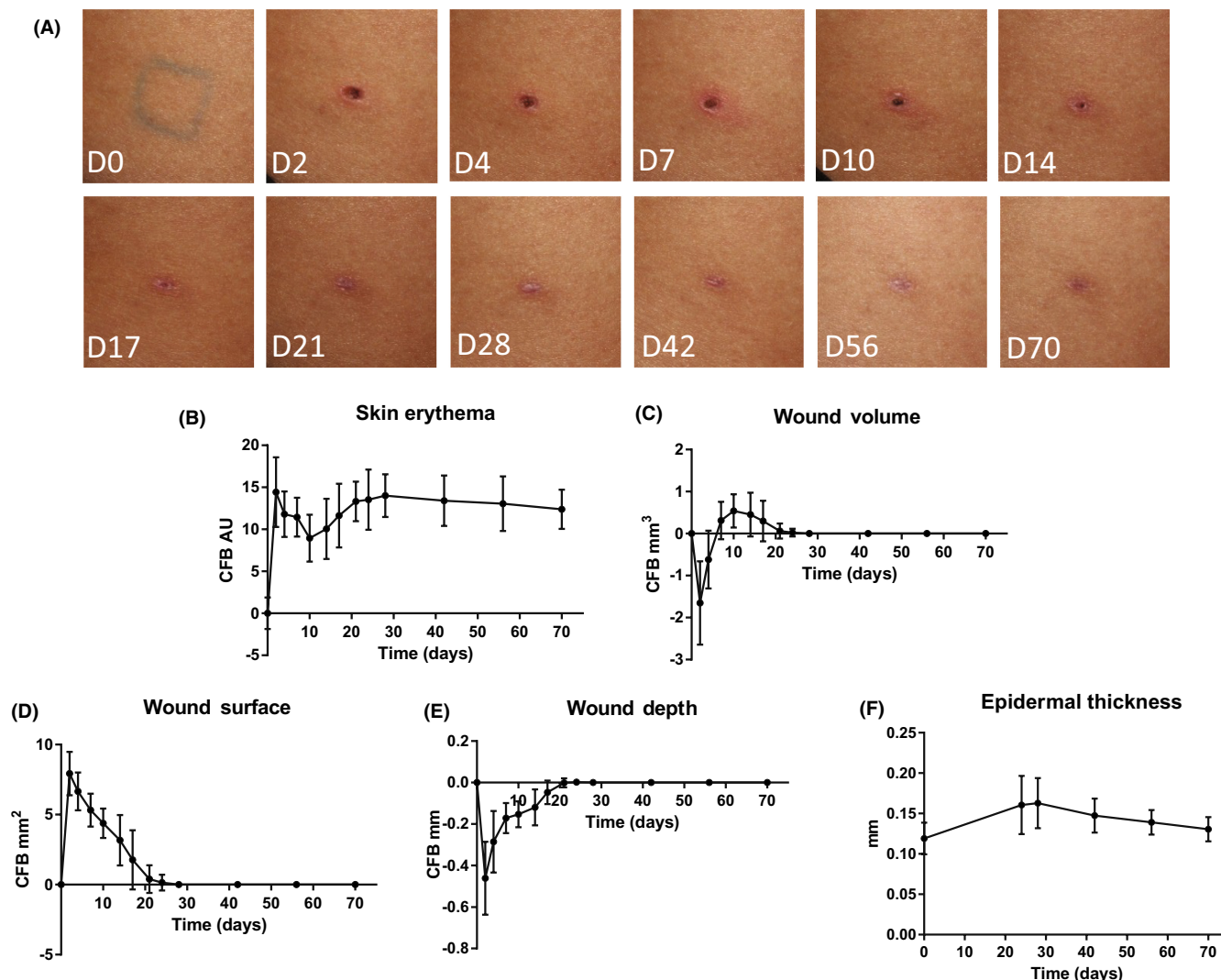


**FIGURE 3** Wound planimetry and clinical imaging. (A) Representative images of wound healing progression over time (photos taken at indicated days). (B) Skin erythema, displayed as change from baseline arbitrary units over time ( $n=18$ ). (C–E) Volume, surface and depth displayed in change from baseline  $\text{mm}^3$ ,  $\text{mm}^2$  and  $\text{mm}$ , respectively ( $n=18$ ). (F) Automatically calculated epidermal thickness displayed in  $\text{mm}$  over time ( $n=18$ ). Data on day 0 is epidermal thickness calculated pre-biopsy procedure. Figures A–E are expressed as means  $\pm$  standard deviation. Figure F is expressed as means  $\pm$  standard deviation.

proteins that are thought to be involved in the proliferation (Phase III) and remodeling phase (Phase IV) of wound healing (i.e. PGF, TGF $\beta$ 1, TGF $\beta$ 3, MMP1, MMP3, MMP9) were already upregulated at day 7. Interestingly, TGF- $\beta$ 3 remained increased up to day 70. All other parameters showed a gradual decrease over time or a plateau at the end of the observational period, Figure 4.

### 3.4 | Histology scores aligned to wound healing phases

Histopathology scoring was performed for each biopsy. Only in case the biopsy was fragmented and/or scoring was not applicable no score was given. Figures S1–S5 display all histology scores. Complete re-epithelialization (Phase III, Figure S1) was achieved on

day 14 for all biopsies. As of day 28, all epithelization parameters returned to pre-wounded skin.

Inflammation scores (Phase II, Figure S2) were divided in three categories (neutrophils, histiocytes, lymphocytes) and an overarching parameter 'total inflammation'. For two biopsies, signs of inflammation were already observed on day 0. On day 7, all biopsies that could be assessed showed scant signs of inflammation, which changed to moderate inflammation in some biopsies and returned to scant after 42 days in most of the biopsies.

Neoangiogenesis (sign of Phase II/III, Figure S3) was scored using two characteristics: vessel proliferation and orientation. Vessel proliferation was visible on day 7 in all biopsies and remained mild to moderately present up to day 70. Vessel orientation was primarily vertical on day 14 (4 biopsies). On all other days, vessel orientation was primarily mixed (vertical and horizontal).



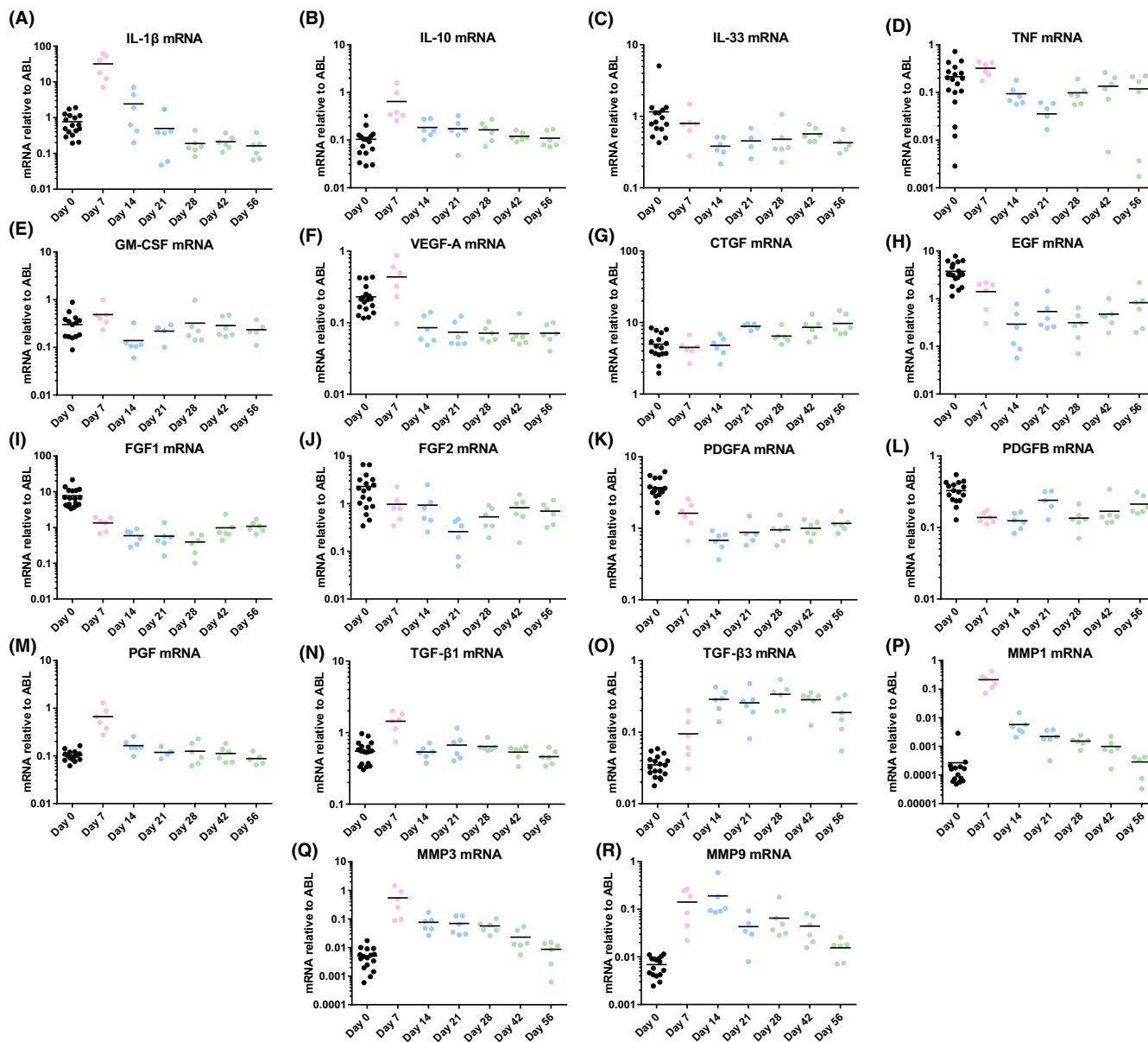


**FIGURE 4** mRNA expressing quantified using qPCR. Data is expressed as individual data points with means, relative to housekeeping gene ABL ( $n = 18$  for day 0,  $n = 6$  for all other timepoints). Colour coding corresponds to wound healing phases depicted in Figure 1A. Black = pre-challenged skin, pink = inflammation phase, blue = proliferation phase, green = remodeling phase. Data are expressed as means.

Granulation tissue (sign of Phase III/IV, Figure S4) was scored using the characteristics: area affected by granulation tissue in % and fibrin deposition. Scant, moderate, profound and excessive correspond to 0%–25%, 25%–50%, 50%–75%, 75%–100% affected, respectively. On day 7, fibrin disposition was profoundly visible and decreased over time up to clearance at day 21. The percentage of area affected was the highest on day 21 and day 28. On day 56 the percentage of area affected differed greatly (2 biopsies scored absent, 4 biopsies scored profound).

Characteristics associated with connective tissue formation (sign of Phase IV) are shown in Figure S5. Proteoglycan/mucin deposition was affected 7 days after wounding. From day 14 onwards, the deposition returned to normal. Elastin deposition remained

unchanged throughout the study. With advancement in time, the amount of collagen deposition fluctuated but was eventually profoundly expressed on day 70. Interestingly, the collagen orientation changed over time from horizontal orientated to mixed orientated. On day 70, 4 biopsies showed horizontal orientation, whereas 2 biopsies showed mixed orientation.

### 3.5 | Data visualization

A complete data visualization using all data described in the preceding sections except epidermal thickness measurements is displayed in Figure S6. The radar chart (Figure S6A) shows involvement of most

parameters for the distinction of phases. The magnitude of pro/anti-inflammatory proteins in the inflammation phase is higher compared to all other phases. In addition, all multidimensional data has been compressed to a one-dimensional t-SNE graph (Figure S6B). The t-SNE plot shows distinct pre-challenged, inflammation, proliferation and remodeling clusters. The figure also illustrates some overlap between the proliferation and remodeling phase. Data points collected from pre-challenged skin and datapoints collected in the inflammation phase shows close clustering and no clear overlap with other phases.

### 3.6 | Non-invasive OCT images vs invasive histology

Figure S7 depicts the progression of wound healing over time as measured by OCT. For comparison, histology slides from day 0, 7, 14, 21, 28, 42, 56 were added to Figure S7, illustrating the different wound healing processes over time (excluding the haemostasis phase, phase I) measured invasively vs non-invasively.

In intact skin (Figure S7A), skin characteristics such as the stratum corneum, epidermis, dermis, dermo-epidermal junction and blood vessels could easily be discriminated in the OCT image.

Phase II (day 2–7): 7 days after wound induction, the first signs of restoration became apparent by a clear haemostatic crust in both the OCT and histology recordings (Figure S7B). In addition, the migrating epidermal tongue originating from the epidermal bulge directly adjacent to the wound and the several dilated perilesional blood vessels were also present as signs of this phase.

Phase III (day 10–24): Complete restoration of the epidermis occurred after 14 days (Figure S7C). In histology, this was shown by an epidermal bulge originating from both perilesional sides of the wound accompanied by a cellular infiltrate. For OCT, the restored epidermis was visualized by a bright white band next to the epidermal bulge caused by the inflammatory infiltrate. Other processes related to the proliferation phase of wound healing were observed 21 days after wounding in both the histology and OCT images (Figure S7D). The epithelium layers were thickened and granulation tissue at the base of the wound was formed.

Phase IV (day 28–70): 28 days after wounding the first processes involved in the remodeling phase of wound healing were seen (Figure S7E). A mixed extracellular matrix orientation was observed in both histological and OCT recordings. In addition, a further flattening of the epidermis was seen. This flattening of the epidermis continued up to day 42 after wounding (Figure S7F). The epidermis was thickened compared to unwounded skin and no rete ridges were visible. Furthermore, a thickening in the upper epithelium layers was seen in the histology recording. The orientation of blood vessels was mixed (horizontal and vertical) but less in density compared to unwounded skin. 56 (Figure S7G) and 70 (Figure S7H) days after wounding, the skin showed increased roughness (on OCT recordings) indicating a less dense extracellular matrix compared to 42 days post wounding. 70 days after wounding, the epidermis was still thickened

compared to unwounded skin (Figure S7A, OCT graph) and showed clear signs of fibrosis (hyperreflective dermis).

### 3.7 | Clinical scores are consistent with clinical imaging

EGS and RYB scores were performed on all study day visits. POSAS scores were performed from the day that the wound was closed (day 14). Data on the scores in frequency over time are displayed in Figure S8. A shift from severe (day 2–10, phase II/III) to moderate (day 14–28, phase III/IV) to mild (day 42–70, phase IV) erythema was observed in the EGS scores. The RYB scores shifted from black to no wound (wound closure) from day 14 onwards. POSAS scorings showed a steep decrease from day 14 up to day 28. A plateau was formed from day 28 to day 70. The scores did not return to the minimal scores of a POSAS score.

## 4 | DISCUSSION

In this study, we aimed to characterize physiological wound healing with a multimodal test battery consisting mainly of non-invasive methodologies in a healthy volunteer challenge model. We demonstrate for the first time that a test battery of non-invasive techniques can objectively monitor quantifiable changes over time of the distinct wound healing phases, that is phase II inflammation, phase III proliferation and phase IV remodeling, while excluding the haemostasis phase. Additionally, multiple parameters were integrated and visualized in a radar chart highlighting the most important parameters and most suitable biomarkers per phase. Lastly, data integration of all parameters by means of t-SNE showed clear clusters per phase. Remarkably pre-challenged skin and the inflammation phase were the most pronounced clusters.

### 4.1 | Clinical imaging as objective read-out for wound healing assessment

Clinical imaging of cutaneous disorders in dermatology is often performed for treatment efficacy evaluation over time.<sup>38</sup> Recent advancements in imaging techniques allows for quantitative and objective measurements to be performed over time without the need for subjective clinical scoring.<sup>39</sup> Using clinical (3D)-imaging we were able to collect objective data on differences over time for 5 characteristics, that is erythema, volume, surface, depth, epidermal thickness. In the observational period, of this study, skin erythema never returned to baseline indicating that the remodeling phase continues for much longer than 70 days.<sup>40</sup> Changes observed in stereophotogrammetric parameters (volume, surface and depth) were in line with known literature on wound closure times. Despite the haemostatic crust covering the wound, the 3D camera used in this study was still able to detect differences in wound surface and depth. For

wound volume, an arbitrary elevation was observed. This was partly accounted for the period a haemostatic crust was present and partly due to skin elevation due to fibrosis.

To summarize, all imaging techniques were able to objectively characterize the phases of wound healing and offer many advantages for both the clinic and in clinical research. One of the biggest advantages is that with these techniques serial non-invasive measurements can be performed on lesions providing objective data over time. Invasive biopsies can only be taken on a limited basis, whilst non-invasive techniques can be used any time. These techniques also have some limitations. 3D photography requires a trained operator to draw wound circumference, thereby introducing potential inter-operator variability. In addition, the effect of crust formation on imaging values is unclear and requires caution with interpretation of data.

## 4.2 | Skin barrier function measurements are useful when assessing wound healing

TEWL is a technique often used in pre-clinical and clinical research as an objective measurement for assessing the barrier function. One of the limitations often reported is the variability of the technique due to fluctuations in humidity, temperature, anatomical site and sweat.<sup>41</sup> In this study, TEWL values decreased over time, that is representing the progression of healing, while maintaining a constant and low variability between subjects. Potential reasons why TEWL values in this study were more robust compared to literature are the use of a temperature-controlled room, standardized measurement setup, a fixed operator, acclimatation time and routine calibration of equipment. TEWL values were increased up to 3 weeks after wounding, which is fully aligned with the time needed for keratinocytes to migrate the epidermis as seen in autoradiographic analysis of unaffected epidermal skin from psoriasis, mycosis fungoides and basal cell carcinoma patients.<sup>42,43</sup> In the current study no dressing was applied after haemostasis was achieved. The question remains whether the TEWL profile over time will remain the same with occlusive dressing in place. It is known from literature that dressing plays a vital role in wound management and future research should include skin barrier measurements using multiple wound dressing protocols.<sup>44</sup>

## 4.3 | Frequent, in-depth molecular profiling of wound healing phases

qPCR analysis performed in this study provided a comprehensible mechanistic insight into the molecular processes at play during wound healing. IL-10, IL-1 $\beta$ , IL-33, TNF, GM-CSF were all upregulated in the first days biopsies were taken (day 0, day 7) indicating on a role in the haemostasis and inflammation phase, which is in line with literature.<sup>45,46</sup> Interestingly, differences over time were observed between TGF- $\beta$ 1 and TGF- $\beta$ 3. This group of growth factors is known

to be involved in both inflammation and proliferation phases and are believed to activate similar intracellular signalling pathways.<sup>47</sup> However, we found that TGF- $\beta$ 1 was only elevated up until 7 days after wounding, whilst TGF- $\beta$ 3 was increased up to day 56 (reaching a plateau on day 14). Wang et al. showed that hypertrophic derived fibroblasts and scar tissue produced more TGF- $\beta$ 1 compared to normal wound healing, indicating that prolonged elevation of TGF- $\beta$ 1 leads to more scarring.<sup>48</sup> Ferguson et al. discovered that skin wounds in mammalian embryos heal without scarring. Notably, TGF- $\beta$ 3 is elevated in these embryos, implying that TGF- $\beta$ 3 has anti scarring properties.<sup>49</sup> Another interesting find was the decrease in several growth factor genes (EGF, FGF1, FGF2, PDGFA, PDGFB) after wounding. For PDGF it is known from literature that it is up-regulated early after wounding.<sup>50</sup> However, in the current study we observed a decrease in these growth factors 7 days after wounding and no return to baseline within 70 days. The first timepoint that post-biopsy samples were taken was after 7 days, which might be after an elevation in growth factors in the early days (2–6 days). In the literature a short and steep elevation of PDGF has been reported.<sup>6,50</sup> After the decrease at day 7 a slight elevation over time occurred, which was insufficient to return to baseline within the 70 days study period. For the MMPs, and in particular MMP-1, we observe a steep increase 7 days after wounding and a slow return to baseline. This is consistent with literature suggesting high levels of MMP-1 one day after wounding followed by a slow return to baseline.<sup>51</sup> Furthermore, we observed that growth factor levels increase slightly over time but that the time course of the study was insufficient to capture a return to baseline of these genes. Even though the goal of this study was to characterize normal wound healing without intervention and no unexpected findings were anticipated, we did not foresee IL-6 to only yield zero values in the qPCR analysis (data not shown). A potential explanation for this could be an analytical assay issue given that all other tested proteins yielded quantifiable levels and no other explanation could be found. IL-6 is known to play a vital part in inflammation and activates both innate and the adaptive immune system.<sup>52</sup> In addition, it is known from literature that IL-6 gene expression is elevated in reepithelization of human skin wounds.<sup>53</sup> Therefore, it was expected that IL-6 would be elevated following the biopsy procedure.

## 4.4 | Integrated, multidimensional data visualization shows distinct wound healing phases

We also assessed if integration of all the objective measures could function as a tool to distinguish healing phases and indicate the most important parameters in a certain phase, indicating the most suitable biomarkers per healing phase. Based on a radar plot, it can be concluded that important distinguishing biomarkers in all phases were wound depth, wound volume and mRNA expression of TGF $\beta$ 3 in the skin punch biopsy. Most of the biomarkers were primarily affected in the inflammation phase indicating that the modalities used in the study are well capable of detecting

differences in this phase. Interestingly, some biomarkers (i.e. IL-33, FGF1, PGF) were only affected in one of the phases showing good distinguishing power of this biomarker. Due to the non-linearity of the data the decision was made to visualize the integration of data using t-SNE. From this t-SNE plot a clear clustering of phases was seen. Pre-challenged skin showed the clearest demarcation compared to the other phases. This is consistent with expectations since all the data used for the integration model showed the biggest differences from day 0 to day 2. Interestingly, data points associated with the proliferation and maturation phases were closest to each other, indicating that there is a partial overlap of processes in the proliferation phase and remodeling phase. Although this visualization of the data suggests that the modalities can be used to distinguish in what phase a certain wound is, it should be interpreted with caution. The time points assignment to the different phases are based on literature and visual assessment of the investigators creating a selection bias.

#### 4.5 | OCT as novel tool for non-invasive wound characterization

OCT has previously been used to visualize and quantify the microcirculation of the skin.<sup>54-56</sup> Vessel density in blister wounds using OCT has been quantified by Larsen et al. and this research group has been able to correlate (albeit weakly) the vessel density measurements with the inflammatory reaction scored using histology.<sup>57</sup> The visualization by OCT in this study showed distinct vasodilatation in the first days after wounding followed by an inwards perfusion on day 14 hinting towards neoangiogenesis inside the wound bed, therewith confirming the applicability of OCT measurements for characterization of the inflammatory status of the skin. OCT has not been frequently used in the field of dermatology for the evaluation of skin morphology. The majority of studies that have been performed were in small populations, focused on few endpoints or were performed in animal models.<sup>58-60</sup> In this study, we confirm applicability of the OCT not only for inflammatory characteristics but also morphological characteristics, allowing a full non-invasive characterization of the wound healing process. OCT images matched the histology recordings regarding the detectability of distinct cutaneous shapes. Restoration of the epidermis, dilatation of blood vessels, granulation tissue and thickening and flattening of the epidermis could all be clearly characterized using OCT. However, despite being able to distinguish cutaneous structures and changes in the microenvironment, OCT also has some limitations. It does not have the diagnostic power and resolution needed to detect all wound healing processes and small micro-environmental changes without the need for histology comparison. In addition, the technique requires trained operators to reduce the number of artefacts in scans. Despite all these limitations the future of the technique looks promising. With recent advancements in resolution, measuring depth, image analysis and standardization of measurement the technique holds promise to replace the need for invasive skin biopsies and become a standard diagnosis tool.<sup>61</sup>

Our study is a first step towards a complete model for adequate drug and device testing in wound healing. These results contribute to a better understanding of the inflammatory responses in the skin's microenvironment. Although the results appear promising, some aspects could be optimized to increase sensitivity and improve the distinguishing power of the non-invasive imaging modalities. The first days of acute wound healing are vital in predicting time to closure and to monitor the first processes in the inflammation phase. Due to the bleeding period in the haemostasis phase, it is difficult to image the wounds shortly after wounding. In hindsight an extra visit 1 day after wounding would have been useful in determining the maximum response (i.e. skin blood perfusion, TEWL). Another addition that could be useful in evaluating wound healing would be the clinical scoring of re-epithelialization and contraction, to explicitly compare with objective endpoints. The wounds induced in this study were small, acute and self-resolving punch biopsies, which reflects the normal wound healing of acute sterile wounds and comparability with chronic, slow healing wounds should be further explored. In addition, the size and location of the wounds are important factors influencing wound healing and should be considered when extrapolating results to a different setting. Lastly, future research should be focused on including intervention as positive and negative controls to better assess the usability of the model in drug and device testing.

## 5 | CONCLUSION

We successfully developed a rapid, quantitative human wound healing model by using a multimodal approach. Clinical imaging, biophysical and non-invasive morphological read-outs were fully concordant with histology and clinical scoring. Future use of the model together with test battery will enable early proof-of-concept of novel wound healing treatments using a homogeneous healthy study population.

### AUTHOR CONTRIBUTIONS

Robert Rissmann, Mahdi Saghari, Martijn B. A. van Doorn and Tessa Niemeyer-van der Kolk conceptualized the study. Wouter ten Voorde, Mahdi Saghari, Jiry Boltjes designed the study and coordinated the research under supervision of Robert Rissmann. Wouter ten Voorde, Mahdi Saghari, Thomas P. Buters, Jiry Boltjes performed clinical operations. Wouter ten Voorde, Marieke L. de Kam, Ahnjili Zhuparris, Jiry Boltjes, Jeffrey Damman analysed the data. Wouter ten Voorde, Mahdi Saghari, Tessa Niemeyer-van der Kolk, Thomas P. Buters, Matthijs Moerland and Robert Rissmann wrote the manuscript. All authors provided feedback and helped writing and finalizing the manuscript.

### ACKNOWLEDGEMENTS

We would like to thank all healthy volunteers who have participated in this study and Cutanea Life Science, Inc., Wayne Pennsylvania, USA for the funding.

## FUNDING INFORMATION

This research was funded by Cutanea Life Science, Inc., Wayne Pennsylvania, USA.

## CONFLICT OF INTEREST STATEMENT

GF was employee of Cutanea Life Science, Inc. at study conduct. All other authors declare no conflict of interest.

## DATA AVAILABILITY STATEMENT

The data supporting the figures and tables in this article are available upon request.

## INSTITUTIONAL REVIEW BOARD STATEMENT

The study was conducted in accordance with the Declaration of Helsinki and approved by the Ethics Committee Stichting Beoordeling Ethiek Biomedisch Onderzoek (CHDR1736, 09OCT2017).

## INFORMED CONSENT STATEMENT

Informed consent was obtained from all subjects involved in the study.

## ORCID

Wouter ten Voorde  <https://orcid.org/0000-0001-7241-2889>

Mahdi Saghari  <https://orcid.org/0000-0002-3829-0037>

Ahnjili Zhuparris  <https://orcid.org/0000-0002-1413-1648>

Thomas P. Buters  <https://orcid.org/0000-0002-6751-5370>

Errol P. Prens  <https://orcid.org/0000-0002-8158-660X>

Jeffrey Damman  <https://orcid.org/0000-0001-5997-7551>

Tessa Niemeyer-van der Kolk  <https://orcid.org/0000-0002-3221-1609>

<https://orcid.org/0000-0002-3221-1609>

Jacobus Burggraaf  <https://orcid.org/0000-0001-7912-0918>

Martijn B. A. van Doorn  <https://orcid.org/0000-0003-1672-7899>

Robert Rissmann  <https://orcid.org/0000-0002-5867-9090>

## REFERENCES

- Singer AJ, Clark RAF. Cutaneous wound healing. *N Engl J Med*. 1999;341(10):738-746. doi:10.1056/NEJM199909023411006
- Akbik D, Ghadiri M, Chrzanowski W, Rohanizadeh R. Curcumin as a wound healing agent. *Life Sci*. 2014;116(1):1-7. doi:10.1016/j.lfs.2014.08.016
- Agren MS, Karlsmark T, Hansen JB, Rygaard J. Occlusion versus air exposure on full-thickness biopsy wounds. *J Wound Care*. 2001;10(8):301-304. doi:10.12968/JOWC.2001.10.8.26109
- Theoret C, Schumacher J. Physiology of wound healing. *Equine Wound Manage*. 2016;9:1-13. doi:10.1002/9781118999219.CH1
- Apfel SC. Nerve growth factor for the treatment of diabetic neuropathy: what went wrong, what went right, and what does the future hold? *Int Rev Neurobiol*. 2002;50:393-413. doi:10.1016/s0074-7742(02)50083-0
- Werner S, Grose R. Regulation of wound healing by growth factors and cytokines. *Physiol Rev*. 2003;83(3):835-870. doi:10.1152/physrev.2003.83.3.835
- Sorg H, Tilkorn DJ, Hager S, Hauser J, Mirastschijski U. Skin wound healing: an update on the current knowledge and concepts. *Eur Surg Res*. 2017;58(1-2):81-94. doi:10.1159/000454919
- Ashrafi M, Xu Y, Muhamadali H, et al. A microbiome and metabolic signature of phases of cutaneous healing identified by profiling sequential acute wounds of human skin: an exploratory study. *PLoS One*. 2020;15(2):e0229545. doi:10.1371/JOURNAL.PONE.0229545
- Landén NX, Li D, Ståhle M. Transition from inflammation to proliferation: a critical step during wound healing. *Cell Mol Life Sci*. 2016;73(20):3861-3885. doi:10.1007/s00018-016-2268-0
- Demidova-Rice TN, Hamblin MR, Herman IM. Acute and impaired wound healing: pathophysiology and current methods for drug delivery, part 1: normal and chronic wounds: biology, causes, and approaches to care. *Adv Skin Wound Care*. 2012;25(7):304-314. doi:10.1097/01.ASW.0000416006.55218.DO
- Öhnstedt E, Lofton Tomenius H, Vägesjö E, Phillipson M. The discovery and development of topical medicines for wound healing. *Expert Opin Drug Discovery*. 2019;14(5):485-497. doi:10.1080/17460441.2019.1588879
- Zielins ER, Brett EA, Luan A, et al. Emerging drugs for the treatment of wound healing. *Expert Opin Emerg Drugs*. 2015;20(2):235-246. doi:10.1517/14728214.2015.1018176
- A Robust Market Rich with Opportunities: Advanced Wound Dressings. Accessed January 10, 2022. <https://www.pm360online.com/a-robust-market-rich-with-opportunities-advanced-wound-dressings/>
- Sen CK. Human wounds and its burden: an updated compendium of estimates. *Adv Wound Care*. 2019;8(2):39-48. doi:10.1089/WOUND.2019.0946
- Pastar I, Wong LL, Egger AN, Tomic-Canic M. Descriptive vs mechanistic scientific approach to study wound healing and its inhibition: is there a value of translational research involving human subjects? *Exp Dermatol*. 2018;27(5):551-562. doi:10.1111/EXD.13663
- Brölmann FE, Eskes AM, Sumpio BE, et al. Fundamentals of randomized clinical trials in wound care: reporting standards. *Wound Repair Regen*. 2013;21(5):641-647. doi:10.1111/WRR.12087
- Kirsner RS, Margolis DJ, Baldursson BT, et al. Fish skin grafts compared to human amnion/chorion membrane allografts: a double-blind, prospective, randomized clinical trial of acute wound healing. *Wound Repair Regen*. 2020;28(1):75-80. doi:10.1111/WRR.12761
- Greaves NS, Benatar B, Whiteside S, Alonso-Rasgado T, Baguneid M, Bayat A. Optical coherence tomography: a reliable alternative to invasive histological assessment of acute wound healing in human skin? *Br J Dermatol*. 2014;170(4):840-850. doi:10.1111/bjd.12786
- Greaves NS, Iqbal SA, Hodgkinson T, et al. Skin substitute-assisted repair shows reduced dermal fibrosis in acute human wounds validated simultaneously by histology and optical coherence tomography. *Wound Repair Regen*. 2015;23(4):483-494. doi:10.1111/wrr.12308
- Rissmann R, Moerland M, van Doorn MBA. Blueprint for mechanistic, data-rich early phase clinical pharmacology studies in dermatology. *Br J Clin Pharmacol*. 2020;86(6):1011-1014. doi:10.1111/bcp.14293
- Ud-Din S, Bayat A. Non-invasive objective devices for monitoring the inflammatory, proliferative and remodelling phases of cutaneous wound healing and skin scarring. *Exp Dermatol*. 2016;25(8):579-585. doi:10.1111/exd.13027
- Jacobse J, ten Voorde W, Tandon A, et al. Comprehensive evaluation of microneedle-based intradermal adalimumab delivery vs. subcutaneous administration: results of a randomized controlled clinical trial. *Br J Clin Pharmacol*. 2021;87(8):3162-3176. doi:10.1111/BCP.14729
- Saghari M, Gal P, Ziagos D, et al. A randomized controlled trial with a delayed-type hypersensitivity model using keyhole limpet haemocyanin to evaluate adaptive immune responses in man. *Br J Clin Pharmacol*. 2021;87(4):1953-1962. doi:10.1111/BCP.14588
- Themstrup L, Ciardo S, Manfredi M, et al. In vivo, micro-morphological vascular changes induced by topical brimonidine



- studied by Dynamic optical coherence tomography. *J Eur Acad Dermatol Venereol*. 2016;30(6):974-979. doi:10.1111/jdv.13596
25. Buters TP, Hameeteman PW, Jansen IME, et al. Intradermal lipopolysaccharide challenge as an acute in vivo inflammatory model in healthy volunteers. *Br J Clin Pharmacol*. 2021;88:680-690. doi:10.1111/BCP.14999
  26. Ly BCK, Dyer EB, Feig JL, Chien AL, Del Bino S. Research techniques made simple: cutaneous Colorimetry: a reliable technique for objective skin color measurement. *J Invest Dermatol*. 2020;140(1):3-12.e1. doi:10.1016/j.jid.2019.11.003
  27. Rijsbergen M, Pagan L, Niemeyer-van der Kolk T, et al. Stereophotogrammetric three-dimensional photography is an accurate and precise planimetric method for the clinical visualization and quantification of human papilloma virus-induced skin lesions. *J Eur Acad Dermatol Venereol*. 2019;33(8):1506-1512. doi:10.1111/JDV.15474
  28. van der Kolk T, Assil S, Rijneveld R, et al. Comprehensive, multimodal characterization of an Imiquimod-induced human skin inflammation model for drug development. *Clin Transl Sci*. 2018;11(6):607-615. doi:10.1111/CTS.12563
  29. Cuzzell JZ. The new RYB color code. *Am J Nurs*. 1988;88(10):1342-1346. doi:10.2307/3470923
  30. Tan J, Liu H, Leyden JJ, Leoni MJ. Reliability of clinician erythema assessment grading scale. *J Am Acad Dermatol*. 2014;71(4):760-763. doi:10.1016/j.jaad.2014.05.044
  31. Chae JK, Kim JH, Kim EJ, Park K. Values of a patient and observer scar assessment scale to evaluate the facial skin graft scar. *Ann Dermatol*. 2016;28(5):615-623. doi:10.5021/AD.2016.28.5.615
  32. Van Der Maaten L, Hinton G. Visualizing data using t-SNE. *J Mach Learn Res*. 2008;9:2579-2605.
  33. Rasche H. Haemostasis and thrombosis: an overview. *Eur Hear J Suppl*. 2001;3(suppl\_Q):Q3-Q7. doi:10.1016/S1520-765X(01)90034-3
  34. Versteeg HH, Heemskerk JWM, Levi M, Reitsma PH. New fundamentals in hemostasis. *Physiol Rev*. 2013;93(1):327-358. doi:10.1152/PHYSREV.00016.2011
  35. Midwood KS, Williams LV, Schwarzbauer JE. Tissue repair and the dynamics of the extracellular matrix. *Int J Biochem Cell Biol*. 2004;36(6):1031-1037. doi:10.1016/J.BIOCEL.2003.12.003
  36. Chang HY, Sneddon JB, Alizadeh AA, et al. Gene expression signature of fibroblast serum response predicts human cancer progression: similarities between tumors and wounds. *PLoS Biol*. 2004;2(2):E7. doi:10.1371/JOURNAL.PBIO.0020007
  37. Pedregosa F, Varoquaux G, Gramfort A, et al. Scikit-learn: machine learning in python. *J Mach Learn Res*. 2011;12:2825-2830. Accessed January 5, 2022. <http://scikit-learn.sourceforge.net>
  38. Kaliyadan F, Manoj J, Venkitakrishnan S, Dharmaratnam A. Basic digital photography in dermatology. *Indian J Dermatol Venereol Leprol*. 2008;74(5):532-536. doi:10.4103/0378-6323.44334
  39. Hibler B, Qi Q, Rossi A. Current state of imaging in dermatology. *Semin Cutan Med Surg*. 2016;35(1):2-8. doi:10.12788/j.sder.2016.001
  40. Gonzalez ACDO, Andrade ZDA, Costa TF, Medrado ARAP. Wound healing—a literature review. *An Bras Dermatol*. 2016;91(5):614-620. doi:10.1590/abd1806-4841.20164741
  41. Alexander H, Brown S, Danby S, Flohr C. Research techniques made simple: Transepidermal water loss measurement as a research tool. *J Invest Dermatol*. 2018;138(11):2295-2300.e1. doi:10.1016/J.JID.2018.09.001
  42. Silverman RA, Lender J, Elmetts CA. Effects of occlusive and semi-occlusive dressings on the return of barrier function to transepidermal water loss in standardized human wounds. *J Am Acad Dermatol*. 1989;20(5):755-760. doi:10.1016/S0190-9622(89)70086-4
  43. Weinstein GD, Van Scott EJ. Autoradiographic analysis of turnover times of normal and psoriatic epidermis. *J Invest Dermatol*. 1965;45(4):257-262. doi:10.1038/JID.1965.126
  44. Bishop A. Wound assessment and dressing selection: an overview. *Br J Nurs*. 2021;30(5):S12-S20. doi:10.12968/BJON.2021.30.5.S12
  45. Dinarello CA. Overview of the IL-1 family in innate inflammation and acquired immunity. *Immunol Rev*. 2018;281(1):8-27. doi:10.1111/IMR.12621
  46. Lim JY, Choi BH, Lee S, Jang YH, Choi JS, Kim YM. Regulation of wound healing by granulocyte-macrophage colony-stimulating factor after vocal fold injury. *PLoS One*. 2013;8(1):e54256. doi:10.1371/JOURNAL.PONE.0054256
  47. Roberts AB, Sporn MB. Differential expression of the TGF-beta isoforms in embryogenesis suggests specific roles in developing and adult tissues. *Mol Reprod Dev*. 1992;32(2):91-98. doi:10.1002/MRD.1080320203
  48. Wang R, Ghahary A, Shen Q, Scott PG, Roy K, Tredget EE. Hypertrophic scar tissues and fibroblasts produce more transforming growth factor-beta1 mRNA and protein than normal skin and cells. *Wound Repair Regen*. 2000;8(2):128-137. doi:10.1046/J.1524-475X.2000.00128.X
  49. Ferguson MW, Duncan J, Bond J, et al. Prophylactic administration of avotermin for improvement of skin scarring: three double-blind, placebo-controlled, phase I/II studies. *Lancet*. 2009;373(9671):1264-1274. doi:10.1016/S0140-6736(09)60322-6
  50. Breuing K, Andree C, Helo G, Slama J, Liu PY, Eriksson E. Growth factors in the repair of partial thickness porcine skin wounds. *Plast Reconstr Surg*. 1997;100(3):657-664. doi:10.1097/00006534-199709000-00018
  51. Caley MP, Martins VLC, O'Toole EA. Metalloproteinases and wound healing. *Adv Wound Care*. 2015;4(4):225-234. doi:10.1089/WOUND.2014.0581
  52. Johnson BZ, Stevenson AW, Prêle CM, Fear MW, Wood FM. The role of IL-6 in skin fibrosis and cutaneous wound healing. *Biomedicine*. 2020;8(5):101. doi:10.3390/BIOMEDICINES8050101
  53. Ågren MS, Litman T, Eriksen JO, Schjerling P, Bzorek M, Gjerdrum LMR. Gene expression linked to reepithelialization of human skin wounds. *Int J Mol Sci*. 2022;23(24):15746. doi:10.3390/IJMS232415746/S1
  54. Glios GD, Verne SH, Aldahan AS, et al. Optical coherence tomography for assessment of epithelialization in a human ex vivo wound model. *Wound Repair Regen*. 2017;25(6):1017-1026. doi:10.1111/WRR.12600
  55. Yuan Z, Zakhaleva J, Ren H, Liu J, Chen W, Pan Y. Noninvasive and high-resolution optical monitoring of healing of diabetic dermal excisional wounds implanted with biodegradable in situ gelable hydrogels. *Tissue Eng Part C Methods*. 2010;16(2):237-247. doi:10.1089/ten.TEC.2009.0152
  56. Holmes J, Schuh S, Bowling FL, Mani R, Welzel J. Dynamic optical coherence tomography is a new technique for imaging skin around lower extremity wounds. *Int J Low Extrem Wounds*. 2019;18(1):65-74. doi:10.1177/1534734618821015
  57. Larsen HF, Ahlström MG, Gjerdrum LMR, et al. Noninvasive measurement of reepithelialization and microvasculature of suction-blister wounds with benchmarking to histology. *Wound Repair Regen*. 2017;25(6):984-993. doi:10.1111/WRR.12605
  58. Cobb MJ, Chen Y, Underwood RA, Usui ML, Olerud J, Li X. Noninvasive assessment of cutaneous wound healing using ultrahigh-resolution optical coherence tomography. *J Biomed Opt*. 2006;11(6):064002. doi:10.1117/1.2388152
  59. Wang Z, Pan H, Yuan Z, Liu J, Chen W, Pan Y. Assessment of dermal wound repair after collagen implantation with optical coherence tomography. *Tissue Eng Part C Methods*. 2008;14(1):35-45. doi:10.1089/tec.2007.0285
  60. Welzel J, Lankenau E, Birngruber R, Engelhardt R. Optical coherence tomography of the human skin. *J Am Acad Dermatol*. 1997;37(6):958-963. doi:10.1016/S0190-9622(97)70072-0

61. Ogien J, Levecq O, Cazalas M, et al. Handheld Line-Field Confocal Optical Coherence Tomography for Dermatology. Vol. 11211. 2020: 44–53. doi:[10.1117/12.2545546](https://doi.org/10.1117/12.2545546)

Figure S5

Figure S6

Figure S7

Figure S8

## SUPPORTING INFORMATION

Additional supporting information can be found online in the Supporting Information section at the end of this article.

Figure S1

Figure S2

Figure S3

Figure S4

**How to cite this article:** ten Voorde W, Saghari M, Boltjes J, et al. A multimodal, comprehensive characterization of a cutaneous wound model in healthy volunteers. *Exp Dermatol*. 2023;32:1028-1041. doi:[10.1111/exd.14808](https://doi.org/10.1111/exd.14808)